EASR

Engineering and Applied Science Research

https://www.tci-thaijo.org/index.php/easr/index

Published by the Faculty of Engineering, Khon Kaen University, Thailand

The effect of solution treatment on corrosion behavior of newly nickel free-stainless steel (NFSS-10Mn-16Cr-3Mo-0.2N)-induction melting manufacture

Miftakhur Rohmah*, Faried M. Ridlo**, Yudi N. Thaha, Permana A. Paristiawan and Nisa R. Hakim

Research Center for Metallurgy, Research National and Innovation Agency (BRIN), Banten 15314, Indonesia

Received 10 March 2022
Revised 31 May 2022
Accepted 18 July 2022

Abstract

Nickel-Free Stainless steel (NFSS) was improved as the next generation in biomedical implant alloys. Inappropriate heat treatment or prolonged exposure at high temperatures in NFSS affects the secondary phase formation and harms corrosion resistance. In this study, the effect of cooling rate during solution treatment on the corrosion behavior of NFSS was observed using Polarization and Electrochemical Impedance Spectroscopy (EIS). NFSS-10Mn-16Cr-3Mo-0.2N was melted in Induction Furnace, solution treated at 1050 ℃ for one hour, and quenched in various media: furnace environment, water, brine, and open-air. The NFSS-10Mn-16Cr-3Mo-0.2N has 21.29 points for the %wt Cr equivalent and 5.25 points for the %wt Ni equivalent. The metallographic result confirmed that the microstructure of NFSS-0.2N consists of elongated ferrite and martensite phase. The cooling rate increased, and the average diameter decreased to 0.021 mm. Consequently, the large of passivity zone (*Epass* 94.5 to 497.32 mV in 0.2-2 x 10^{-6} A of *Ipass*) was obtained after furnace cooling. The passivity starts from the passivating species (Cr_2O_3) adsorption on a metal surface and improves corrosion resistance. In addition, slowed cooling sample has lower values of corrosion (-38.2 mV for E*corr*, 0.128 µA/cm^2 for I*corr*, and 1.49x10^{-3} mm/year) and highest value of impedance |Z'|. The Bode plot of EIS shows that the passive film being formed at low frequency and the reduction of cooling rate leads to increasing the arc radii.

Keywords: Corrosion, Hank's solution, NFSS-10Mn-16Cr-3Mo-0.2N, Nickel free-stainless steel, Solution treatment

1. Introduction

The fundamental criterion for choosing a biomedical alloy should provide the necessary mechanical strength, corrosion resistance, and excellent biocompatibility. The suggested metallic implant device is used mainly by stainless steel (AISI 316L), Grade 5 Ti-6Al-4V, and Co-Cr-Mo alloy. Unfortunately, Stainless steel 316L has limitations for corrosion localized such as pitting, crevice, and stress corrosion cracking when corroded in the human body environment for a long time [1]. The corrosion is liable for the release of harmful nickel ions, which carries a mutagenic-genotoxic activity, allergic reaction, and sometimes cancer [2]. Nickel-free stainless steels (NFSS) with lower danger toxicity are believed to be improved as the next generation for replacing 316L.

In recent years, the nitrogen-containing low-Ni have drawn in purposeful development. NFSS is typically produced using an induction furnace, electric arc furnace, pressured electro slag remelting, plasma arc melting, argon oxygen decarburization, and powder metallurgy [1]. Numerous examinations have developed nickel-free stainless steel. Nitrogen-alloying offers extraordinary difficulties since the solubility of nitrogen in liquid Fe-based alloys is exceptionally low under atmospheric pressure, around 0.08 wt.% for ferritic and 0.4 wt.% for austenitic stainless steel [1-2]. Nitrogen advances the stability of the austenite phase without martensite formation during cold-working. Nitrogen is considered an essential alloying addition in austenitic stainless steel to improve the inter-crystalline corrosion resistance. It can enhance the passivation ability and decrease the metastable pitting susceptibility equals to 16 times more excellent, than with Cr addition [3-4]. The cooling rate or alloying elements level seriously affects the microstructure, several secondary phases, plasticity, toughness, and corrosion resistance of stainless steel. However, inappropriate heat treatment or prolonged exposure at elevated temperature in austenitic SS with a high level of nitrogen addition can cause embrittlement by the carbide, nitride precipitate formation, and strain aging, such as δ-ferrite, precipitate (Cr_2N), the x phase (Fe, Cr, Mo intermetallic compound), and the δ phase due to the segregation of Cr, Mo, N, and Mn during casting [4-5]. The presence of these phases will deteriorate the steel properties by making them more susceptible to corrosion.

In general, solution treatment work to obtain a single-phase austenitic structure, prevent secondary phase formation and improve the mechanical properties [6-7]. Control of microstructure during crystallization and solidification plays a crucial role in stainless development and influences its properties. Depending on Cr_{eq}/Ni_{eq} ratio, crystallization is performed, and competitive growth through austenite/δ-ferrite with various mechanisms [8]. The corrosion resistance in NFSS is attributed to the Cr, Mo, and N elements to provide the phase fraction between ferritic and austenitic. Hernandez et al. studied the variation of solution treatment temperature, which is 1010, 1040, 1070, and 1100 ℃, in 17Cr-6Mn-5Ni-1.5Cu and 304L austenitic SS significantly affect the pitting corrosion-resistant and passivity region due to volume fraction of intermetallic phase [9]. Cui et al. also conclude that increased the solution time, the secondary phase decreased, the grain size increased, and the passivity film of Cr_2O_3, Mo^{4+}, and Mo^{6+} oxides is formed chiefly [7]. However, there is little research about the effect of the cooling rate at solution treatment process on corrosion resistance of NFSS. It is notable to find

*Corresponding author. Tel.: +62 857 3032 5042
Email address: mift011@brin.go.id, fari010@brin.go.id
doi: 10.14456/easr.2022.66

optimal solution treatment conditions and study their impact on newly NFSS steel. Herein, an NFSS-10Mn-16Cr-3Mo-0.2N with four cooling mediums of solution treatment is investigated by electrochemical test to clarify the attribute of cooling rate on the corrosion behavior and passive film mechanisms.

2. Materials and methods

2.1 Materials preparation

In this work, the nickel-free-stainless steels have been manufactured using an induction melting furnace (Inductotherm type-100kg in PT. Trieka Aimex, Indonesia) by adding nitride ferroalloy. In stoichiometry conditions, the iron scrap and ferroalloy (ferrochrome, ferromanganese, Mn, Cr) were melted at 1700-1800 ^{o}C and then cast using a Y-block of sand mold. OES Spectrolab confirmed the average chemical composition of NFSS-10Mn-16Cr-3Mo-0.2N cast with triple measurement, which is shown in Table 1.

The NFSS-10Mn-16Cr-3Mo-0.2N cast of 10x20mm was cut using a wire-cut machine from the ingot. The specimen was homogenized at 1100 ^{o}C for 3 hours and open air-cooled. Then, all samples were solution treated at 1050 ^{o}C for 1 hour using a muffle furnace (Nabertherm type LH-15/14"/C440). The difference in cooling media is used for determining the effect of the cooling rate after the solution treatment process. The quenchant is water, brine, and open air.

Table 1 Chemical composition of nickel free-stainless steel

C	Si	Mn	Cr	Ni	Mo	N	Cu	P	S	Fe
0.05	0.38	9.95	16.64	0.15	2.98	0.20	0.31	0.01	<0.0005	Bal

2.2 Characterization

Several stages of specimen preparation for the metallography include the grinding process using sandpaper SiC up to 1200 grit and polishing using 1-micron alumina. After obtaining a glass-like surface, the specimens are etched in aqua regia solution (HCL: HNO_3: H_2O is 3:1:20) for 5 seconds. The microstructures of specimens are observed by optical microscopy (Olympus BX-53M).

A potentiodynamic polarization & EIS test was performed in a typical three-electrode configuration and immersed in a fluid body environment at room temperature. The simulated body fluid is employed in Hank solution, which has the chemical composition in Table 2. The NFSS-10Mn-16Cr-3Mo-0.2N acts as the working electrode, the platinum wire is conducted as the counter electrode, and Ag/AgCl is employed as the reference electrode. Before the test, according to ASTM G61, the NFSS-10Mn-16Cr-3Mo-0.2N was connected with copper wire and grind with SiC paper up to 600 grit for new surface formation. After grinding, The NFSS was subjected to an ultrasonic bath to clean the surface. The Electrochemical impedance spectroscopy (EIS) was performed to measure the impedance of system independence of the AC potentials frequency. The input sinusoidal signal amplitude was 10mV with a sweep frequency from 0.1 Hz to 100kHz-referring to Eocp.

Table 2 Hank solution composition (in g/L)

Composition	Concentration (g/L)
NaCl	8
KCl	0.4
$CaCl_2$	0.14
$MgSO_4.7H_2O$	0.1
$MgCl_2.6H_2O$	0.1
$Na_2HPO_4.2H_2O$	0.06
KH_2PO_4	0.06
$NaHCO_3$	0.35
D-Glucose	1

3. Results and discussion

3.1 Microstructure analysis

Four samples of NFSS-10Mn-16Cr-3Mo-0.2N was cooled down with different cooling condition: furnace, water, brine, and open-air, to study the effect of cooling rate on the phase transformation during solution treatment. The metallography test achieved the microstructure measurement in 20x magnification objective lenses, depicted in Figure 1.

Figure 1 shows the microstructure of nickel-free stainless steel under different cooling conditions is similar and dominated by ferrite (α), martensite (α') as delta ferrite, without a twinning structure and no precipitates present inside grain boundaries. The alloys containing 14% Cr and less than 11% Ni were due to martensite formed on cooling to room temperature. The ferrite phase is respected by bright elongated-island as a matrix, while the martensite phase is distributed irregularly along grain boundaries of the α phase with dark area [10]. In the simple Fe-Cr-Ni stainless steel, ferrite and martensite structures in its alloy are ferromagnetic [2], and martensite has poor ductility. The ferritic phase formed through diffusional transformation, and the martensitic phase with non-diffusional. Based on composition and the calculation of Ni and Cr equivalent (Equation 1-2), this alloy has 21.29 points for %wt. Cr equivalent and %wt. 5.25 points of Ni equivalent, so that when plotted on the Modified Schiffer diagram, it will be in the austenite + martensite + ferrite region [11-12]. The absence of austenite is due to the lack of nitrogen content which is only 0.2% and has not been able to replace the role of nickel in the formation of austenite. The ferrite promoting elements are Cr, Mo, Si, V, Ti, or Al, while the austenite promoting elements are Ni, C, Mn, and N. Chromium (Cr) tends to stabilize α-Fe into Fe-Cr alloys.

$$\text{Ni equivalent} = \text{Ni} + \text{Co} + 0.1\text{Mn} - 0.01\text{Mn}^2 + 18\text{N} + 30\text{C} \quad (1)$$

$$\text{Cr equivalent} = \text{Cr} + 1.5\text{Mo} + 1.5\text{W} + 0.48\text{Si} + 2.3\text{V} + 1.75\text{Nb} + 2.5\text{Al} \quad (2)$$

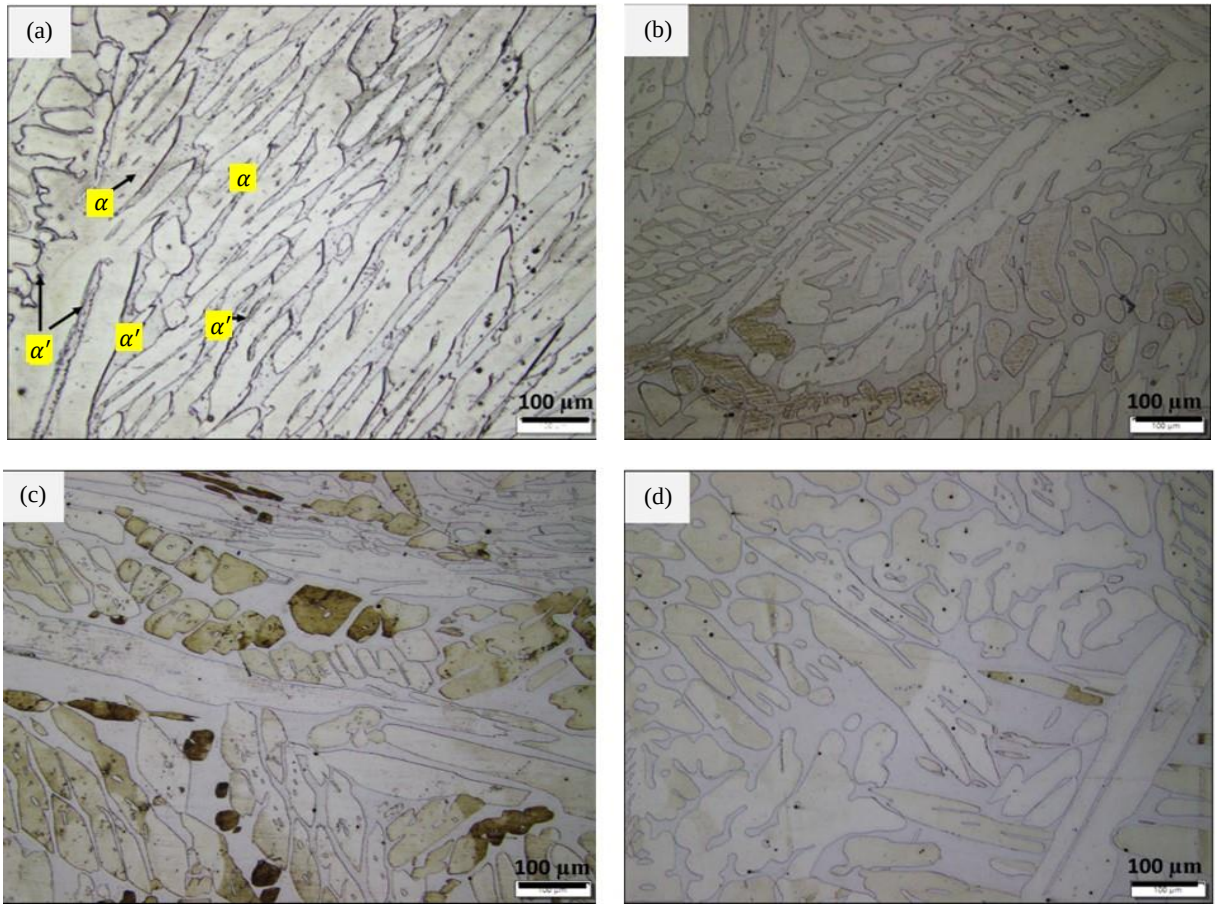

Figure 1 Microstructure of NFSS-10Mn-16Cr-3Mo-0.2N with (a) furnace, (b) water, (c) brine, and (d) air cooling treatment.

Table 3 Microhardness and grain size calculation of NFSS-10Mn-16Cr-3Mo-0.2N

Sample	Ferrite phase hardness (VHN)	Marten site phase hardness (VHN)	ASTM Grain size number (n)	ASTM Grain size number to number of grains (N_M)	Average diameter (mm)
Furnace cooling	253.8±3.27	261.8±3.83	6.051026	82821.19	0.039
Air cooling	246.1±4.75	256.1±2.68	7.603104	242514.7	0.022892
Water cooling	255.4±3.21	267.4±2.41	7.814261	280513.8	0.021277
Brine cooling	261.9±5.32	263.9±4.04	7.781004	274740.9	0.021523

In addition, the cooling medium slightly affects the grain size number, as listed in Table 3. According to the ASTM E-112 standard with the Heyn Intercept method, the grain size calculation shows that increasing the cooling rate decreases the average diameter and number of grains. The average diameter after furnace, open-air, water, and brine cooling are 0.039 mm, 0.022 mm, 0.021 mm, and 0.021 mm, respectively. Faster cooling rates directly induce the full undercooling for γ-phase nucleation and finally lead to finer microstructure. The micro-hardness increases with rapid cooling, i.e., water or brine cooling, is above 250 VHN. However, the cooling conditions affect the transformation temperature, initiating the nucleation at elevated temperature, dissolving chromium-rich in the α' phase, and improving the hardness properties [4].

3.2 XRD Analysis

The crystalline phase structure of low nickel-austenitic stainless was determined using x-ray diffraction. Figure 2(a) shows the X-Ray Diffraction pattern (Co-Kα radiation) for these alloys with a varying cooler of solution treatment. From this figure, the plane of (110), (200), and (211) are interpreted as BCC structure (ferrite phase). While, the (101), (002), and (102) are indicate the α'(BCT) structure (martensite phase) which is consistent with the microstructure in Figure 1. The absence of austenite is due to nitrogen addition in low levels and doesn't replace nickel. Some small peaks indicate the presence of small amounts of iron nitrides ($FeN_{0.095}$), which have a martensitic structure. The peak intensity of the α-phase is higher than α' phase, indicating the result is mainly dominated by ferritic. The XRD result calculated the volume fraction of each phase by Rietveld method in XRD result. The quantity of martensite peaks appears to increase with the cooling rate, as seen in Figure 2(b). As the cooling rate increases, the proportion of γ-phase transformed will decrease. A slower cooling rate gives the γ-phase enough time to change and promote the α-formation.

The α'-martensite can be directly formed from austenite and tend to ferromagnetism as BCT. Tetragonal may occur when the inclusion element distorts the cubic structure. The martensitic transformation is believed to be a displacive transformation without the diffusion of atoms. The nickel content is lower than 0.3% in these alloys, and the austenitic forming elements are usually 9.5-24 wt% Mn and 0.45-1.1 wt.% N, and Mo. Manganese maintains the austenitic phase structure. The combination of Cr, Mn, and N in this steel effectively tends Cr_2O_3 passive film in the inner structure and increase corrosion resistance [13].

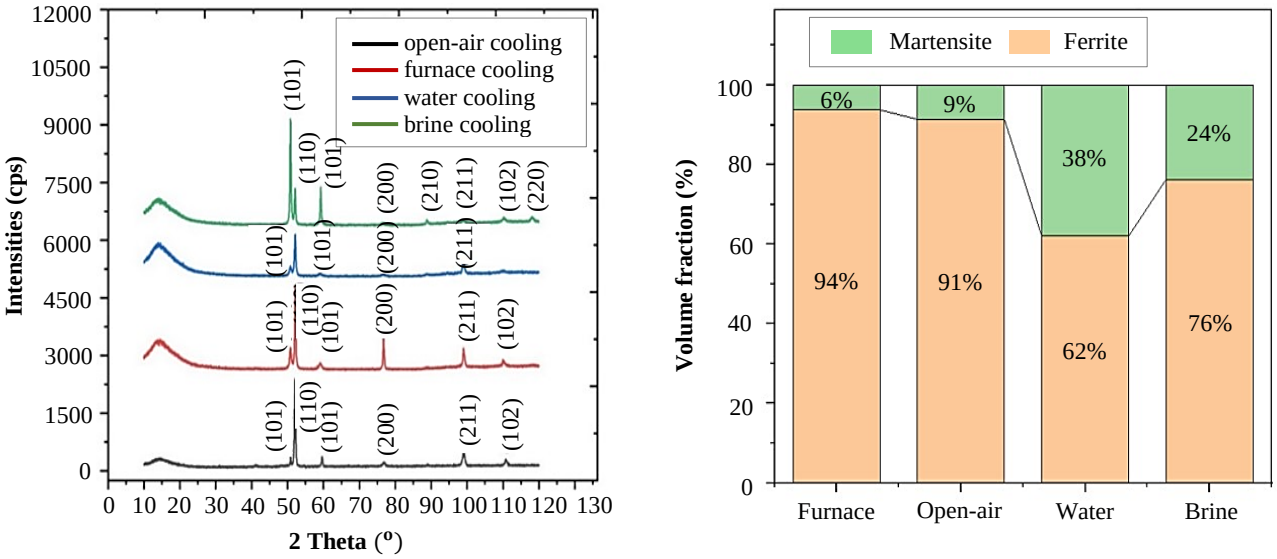

(a) (b)

Figure 2 (a) XRD Pattern (b) Semi-quantitative analysis of phase fraction of low nickel-austenitic stainless

3.3 Polarization analysis

The polarization curves were swept from negative potential, where hydrogen evolution reaction is dominant, towards more positive potential at a scan rate 1 mV/s. The oxidation or reduction are prevalent depending on the direction of polarization on the NFSS-10Mn-16Cr-3Mo-0.2N surface. The potentiodynamic polarization behavior of NFSS in simulated body fluid is depicted in Figure 3. After fitting the curve, the electrochemical critical parameter, including corrosion potentials (E_{corr}), corrosion current (I_{corr}), the passive potentials (E_{pass}), the passive current (I_{pass}), and the widths of passive are summarized in Table 4.

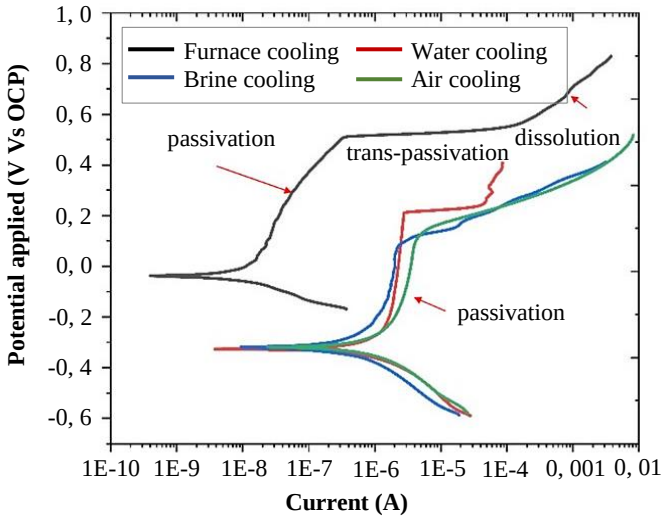

Figure 3 Potentiodynamic polarization curves for NFSS-10Mn-16Cr-3Mo-0.2N in hank solution

Figure 3 demonstrates the effect of cooling media on the anodic behavior of NFSS-10Mn-16Cr-3Mo-0.2N in simulated body fluid. All curves exhibited a mixed control by activation and followed a pseudo-passivation. The spontaneously passivated dan trans-passivated behavior after the anodic activation in nearly constant passivation current density is observed in all samples. The current density is almost constant and proportional to the charge transferred in the passive zone [14]. In this work, the width range of the passivation zone (E_{pass}) is 94.5 to 497.32 mV for furnace cooling at 0.2-2 x 10^{-6} A of current density, -250.05 to 216.37 mV for water cooling at 1.30-2.77 x 10^{-6} A of current density, -205.53 to 75.22 mV for brine cooling at 1.03-2.19 x 10^{-6} of current density, and-235.6 to 93.9 mV for air cooling at 1.61-3.90 x 10^{-6} of current density. It indicates that NFSS-10Mn-16Cr-3Mo-0.2N with furnace cooling has better passivity than brine and air quenched due to the lower volume fraction of the α'-martensite phase. The higher the amount of martensite, the more corrosion reaction is because the carbide in α'-martensite phase might act as cathodic sites. The high passivity film of the NFSS is probably caused by the high concentration of chromium or the existence of nitrogen in surface oxide film during polarizing in Hank [13, 15]. Chromium at minimum content of 13% leads to passivation spontaneously. Mainly, the passive film consists of Fe-rich oxides/hydroxides on the outer and Cr-oxides on the inner surface. The lower current density and more expansive passive zone verified that the passivation could quickly form on the surface and be very stable. The passivity usually starts from the passivating species' adsorption on the metal surface [16].

In addition, a trans-passivation zone indicates a passivated metal starts rapid dissolution, and the potential of the metal becomes too positive, closely related to localized corrosion phenomena. The passive film locally breakdown (E_b) is near 0.5 V, 0.22 V, 0.75 V, and 0.93 V for furnace, water, brine, and air-cooling condition, respectively. The air-cooling sample has better pitting corrosion resistance, reflecting the higher E_b value. It was noted that the pit would initiate and propagate at the surface along with the oxygen evolution and further dissolving of the passive film, which is commonly believed due to the transition of stable Cr^{3+}-oxide to soluble Cr^{6+} species [14].

Table 4 Polarization parameter of NFSS-10Mn-16Cr-3Mo-0.2N in hank solution

Sample code	Ecorr, Obs (V)	Jcorr (A/cm²)	Corrosion rate (mm/year)
Furnace cooling	-0.0382	1.28×10^{-7}	1.49×10^{-3}
Water cooling	-0.327	1.50×10^{-4}	1.7401×10^{-3}
Brine cooling	-0.31951	4.55×10^{-6}	5.28×10^{-2}
Air cooling	-0.31891	9.67×10^{-6}	1.12×10^{-1}

As a result, the corrosion resistance of the furnace cooling sample is superior to the other, which have a corrosion potential more positive but the corrosion current higher than others due to the low content of the α'-martensite phase (6% Vf). The corrosion potential (E_{corr}) is indicated as the energy needed for corrosion reaction in a specific corrosive environment, while the corrosion current density (I_{corr}) illustrates the spontaneous corrosion rate at the corrosion potential [17]. The positive E_{corr} and the lower I_{corr} indicated better corrosion performance. Slowed cooling (furnace and open-air media) sample presented lower values of corrosion which is -38.2 mV for E_{corr}, 0.128 µA/cm² for I_{corr}, and 1.49×10^{-3} mm/year. The polarization curve shifted downward, increasing the cooling rate, and indicating a degraded corrosion resistance. The corrosion decrease can be attributed to $FeN_{0.095}$ formed and the volume fraction between the ferrite and martensite phases [18].

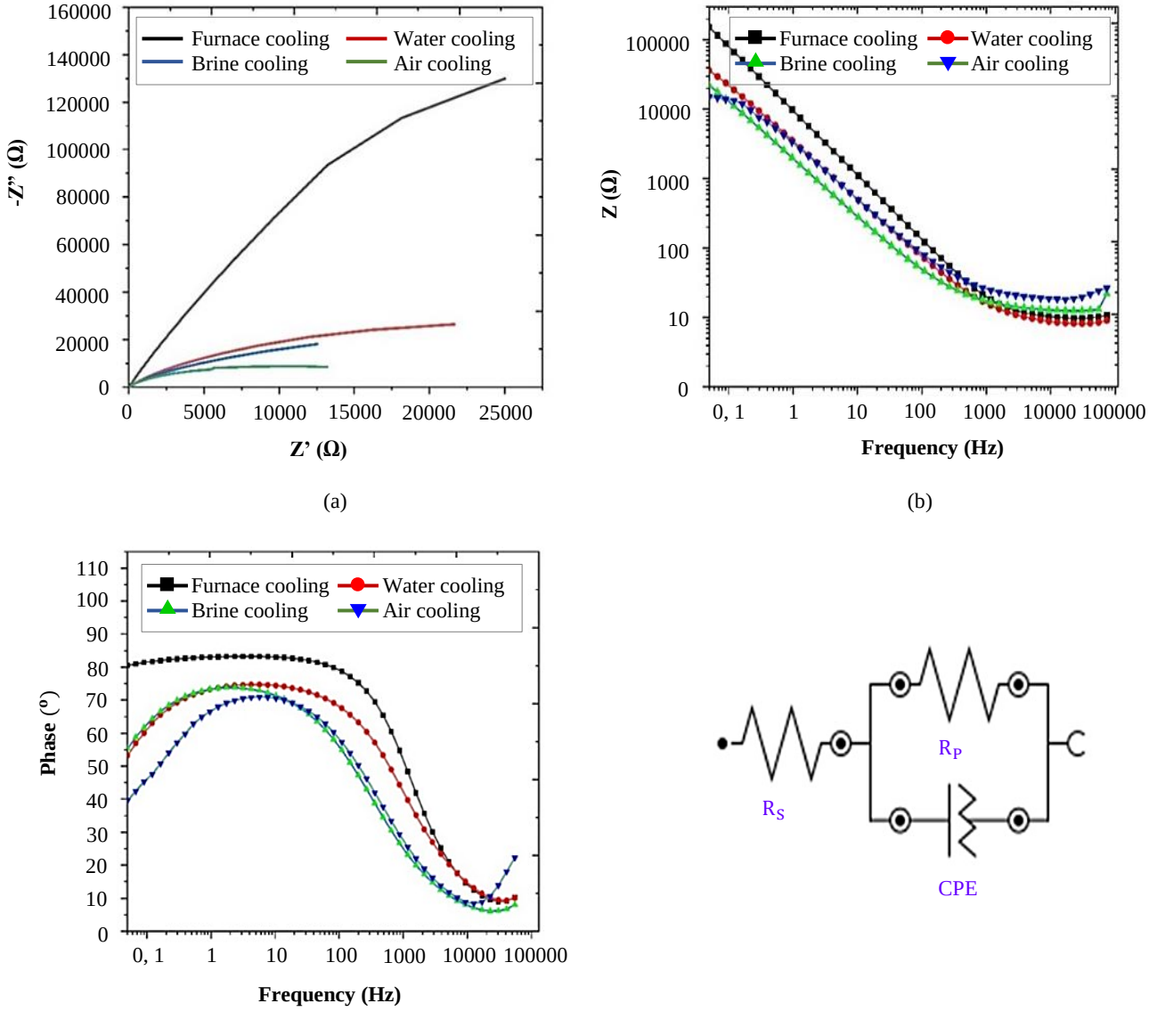

Figure 4 (a) Nyquist, (b) Bode plot, (c) Bode phase, and (d) Equivalent circuit of NFSS-10Mn-16Cr-3Mo-0.2N

An electrochemical impedance of Nyquist and Bode Plot for NFSS-10Mn-16Cr-3Mo-0.2N is performed at 37 ℃ in Hank solution, depicted in Figure 4. The impedance spectra are based on the interfacial reaction at the electrode surface. The EIS parameters, including CPE (constant phase element), Rs (solution resistance), Rp (polarization resistance), characterize the surface layer behavior and are listed in Table 5. The Rs refers to the resistance of Hank's solution, Rp corresponds to the electron charge transfer of resistance, and proportional to corrosion resistance at the passive potential, CPE is related to the double-layer capacitance or the electrical charge transfer at the NFSS alloys/Hank interface.

According to Figure 4(a), the Nyquist plot of all samples shows an impedance of real |Z'| and imaginer |Z"| result with varying visible radius, slope, and size of unfinished semicircles of the impedance curve. The single unfinished semicircle in the capacitive arc refers to the similar complete passivating mechanisms of NFSS-10Mn-16Cr-3Mo-0.2N in the same solution. The slow cooling can increase in |Z'| value of impedance and increase the capacitive arc radii at high frequency, indicating the higher protection improved due to the electron charge-transfer process in the metal surface-electrolyte interface [6, 19]. The corrosion resistance is optimal by furnace cooling and the reduction of cooling rate leads to increasing the arc radii. As shown in Figure 4, the furnace cooling rate has the highest impedance value (approximately 7x more excellent) at all frequencies than the others. The value of Rp of furnace sample is more elevated, 3113.8 kΩ, indicating the corrosion resistance better than others. Higher corrosion resistance can be attributed to the absence of the martensite phase and the effect of grain size, so the release of harmful of nickel ions have prevented during the polarization test [13]. In this experiment, it was assumed that the alloying elements are converted to Fe^{2+}, Cr^{3+} and Ni^{2+} during dissolution. Decrease the cooling rate, the grain size increase (Table 3), the range of passivity potential (E_{pass} in Figure 3) is slightly increased, and the passive film resistance (Rp) increase (Figure 4). The n values are 0.808-0.998, directly related to the electrode roughness and heterogeneities represented as ideal capacitors [20].

Table 5 EIS Fitting parameters obtained from equivalent circuit

Sample	Rs (Ω)	Rp (kΩ)	CPE µMho	N
Furnace cooling	9.481	3113.800	1.02	0.99864
Water cooling	8.349	95.637	62.31	0.8317
Brine cooling	16.884	66.948	47.54	0.9968
Open air cooling	18.83	23.264	73.5	0.80875

Similar tendencies are observable in the Bode plot (Figure 4b-c) for all samples. Bode plot illustrates the resistive response at high frequency (f>100 Hz) and the capacitive behavior in the middle to low frequency (f<10 Hz). The impedance and phase angle drops slightly towards the lower value (Figure 4b) and near-zero degree (Figure 4c) in the high-frequency region, indicating the impedance phase is mainly dominated by *Rp* and shifted to the capacitor as frequency goes low. Under the low frequency, the maximum impedance is above 10^4-10^7 Ω for all samples. From low to medium frequency, the phase angle remains close to ~90°, indicating the typical passive film formed in the surface NFSS-10Mn-16Cr-3Mo-0.2N alloys and preventing the aggressive corrosion species of Hank's solution, respectively. In addition, the maximum phase angle of furnace cooling samples is greater and relatively broader than the other. It can be concluded that the compact passive layer of its sample has an excellent barrier to corrosion and improves the charge transfer resistance at the metal/electrolyte interface [21]. The high frequency is related to the charge-transfer process by double-layer/space charge capacitance, while the low frequency is related to the slower mass-transport process or diffusion of electroactive species for the passive film formation [22].

The best of the electrical equivalent circuits is shown in Figure 4(d), which consists of Capacitor (*CPE*) and resistor (*Rs* and *Rp*) in parallel connection. This circuit was previously proposed by Kim et al. [23]. The capacitance element is the constant phase element (CPE) for the equivalent circuit, which takes the rough NFSS-10Mn-16Cr-3Mo-0.2N of morphology surface and inhomogeneous reaction rate for the capacitive dispersion (Figure 1).

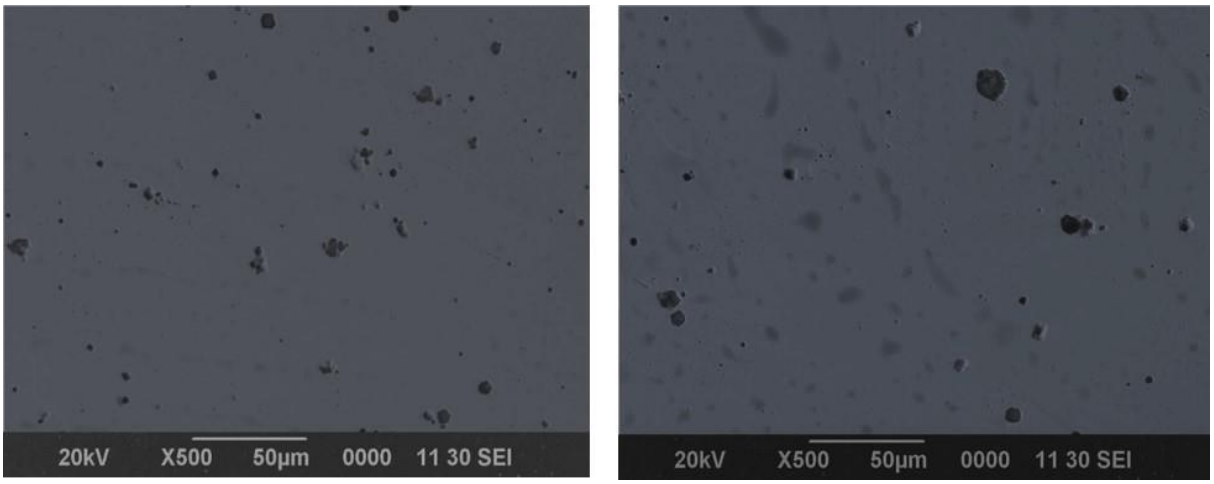

(a) (b)

Figure 5 Surface observation of (a) furnace cooled and (b) water cooled sample after polarization test

The surface morphology after polarization test was conducted by scanning electron microscope (SEM), depicted in Figure 5. Several metastable pits can be observed on the surface of with uniform distribution. As the cooling rate increase, the size of pit increased gradually and the quantity of pits slightly decreased. It indicated that the furnace-cooling sample has higher pitting corrosion resistance.

4. Conclusions

In this work, the electrochemical corrosion behavior of NFSS-10Mn-16Cr-3Mo-0.2N after solution treatment was investigated in a simulation body fluid system using Hank's solution. The varying quenching media in solution treatment affects the microstructure (ferrite and martensite) formation and corrosion behavior. As the cooling rate increase, the martensite (up to 38% of fraction) tends to form along grain boundaries of ferrite so that it affects the polarization behavior and passivation mechanisms after the anodic dissolution. The superior corrosion resistance (around $1.49x10^{-3}$ mm/year) with a broader range of passivation potential (from 94.5 to 497.32 mV) was exhibited by furnace cooling due to Cr_2O_3 passive film formation in the inner layer. From EIS results, the furnace cooling rate has the highest impedance value (3113.8 kΩ) at all frequencies than the others. However, as the cooling rate increase, the size of pit increased gradually and the quantity of pits slightly decreased.

5. Acknowledgements

The material study was funded through the National Priority Project under Deputy for Engineering Science-Indonesian Institute of Sciences (LIPI) in 2020. The facilities, scientific, and technical support from Research Center for Metallurgy and Materials, National Research and Innovation Agency.

6. References

[1] Talha M, Behera CK, Sinha OP. A review on nickel-free nitrogen containing austenitic stainless steels for biomedical applications. Mater Sci Eng C. 2013;33(7):3563-75.
[2] Patnaik L, Maity SR, Kumar S. Status of nickel free stainless steel in biomedical field: a review of last 10 years and what else can be done. Mater Today Proc. 2020;26:638-43.
[3] Feng H, Jiang Z, Li H, Lu P, Zhang S, Zhu H, et al. Influence of nitrogen on corrosion behaviour of high nitrogen martensitic stainless steels manufactured by pressurized metallurgy. Corros Sci. 2018;144:288-300.
[4] Wang T. The effects of cooling rate and alloying elements on the solidification behaviour of continuously cast super-austenitic and duplex stainless steels [thesis]. New South Wales: University of Wallongong; 2019.
[5] Zhou R, Northwood DO, Liu C. On nitrogen diffusion during solution treatment in a high nitrogen austenitic stainless steel. J Mater Res Technol. 2020;9(2):2331-7.
[6] Li J, Shen W, Lin P, Wang F, Yang Z. Effect of solution treatment temperature on microstructural evolution, precipitation behavior, and comprehensive properties in UNS S32750 super duplex stainless steel. Metals. 2020;10(11):1-15.
[7] Cui Y, Qurashi MS, Wang J, Chen T, Bai J, Dong N, et al. Effect of solution treatment on the microstructure and performance of S31254 super austenitic stainless steel. Steel Res Int. 2019;90(8):1-9.
[8] Kazakov AA, Oryshchenko AS, Fomina OV, Zhitenev AI, Vikhareva TV. Controlling behavior of δ-ferrite in nitrogen-containing chromium-nickel-manganese steels. Inorg Mater Appl Res. 2017;8(6):817-26.
[9] Hernández JWC, Ladino DH, Azevedo CRF, Falleiros NA. Effect of solution heat treatment on the pitting corrosion behavior of a high Mn austenitic stainless steel in chloride solution. Rem Rev Esc Minas. 2015;68(1):91-6.
[10] Jang KN, Kim TK, Kim KT. The effect of cooling rates on carbide precipitate and microstructure of 9CR-1MO oxide dispersion strengthened (ODS) steel. Nucl Eng Technol. 2019;51(1):249-56.
[11] Menzel J, Kirschner W, Stein G. High nitrogen containing Ni-free austenitic steels for medical applications. ISIJ Int. 1996;36(7):893-900.
[12] Hull FC. Delta ferrite and martensite formation in stainless steels. Weld Res. 1973;52(5):193-203.
[13] Sun S, Wei S, Wang G, Jiang Z, Lian J, Ji C. The synthesis and electrochemical behavior of high-nitrogen nickel-free austenitic stainless steel. J Mater Eng Perform. 2014;23(11):3957-62.
[14] Eliaz N. Corrosion of metallic biomaterials: a review. Materials (Basel). 2019;12(3):1-91.
[15] Kuroda D, Hiromoto S, Hanawa T, Katada Y. Corrosion behavior of nickel-free high nitrogen austenitic stainless steel in simulated biological environments. Mater Trans. 2002;43(12):3100-4.
[16] Wu X, Fu Y, Ke W, Xu S, Feng B, Hu B. Effects of nitrogen on passivity of nickel-free stainless steels by electrochemical impedance spectroscopy analysis. J Mater Eng Perform. 2015;24(9):3607-14.
[17] Yi G, Liu X, Zheng C, Zhang H, Xu C, Cui YW, et al. Characteristics of passive films formed on as-cast Ti-6Al-4V in Hank's solution before and after transpassivation. Front Mater. 2021;7:1-11.
[18] Cronemberger MER, Nakamatsu S, Della Rovere CA, Kuri SE, Mariano NA. Effect of cooling rate on the corrosion behavior of as-cast SAF 2205 duplex stainless steel after solution annealing treatment. Mater Res. 2015;18:138-42.
[19] Sun Y, Zhao J, Liu L, Xi T, Yang C, Li Q, et al. Passivation potential regulating corrosion resistance and antibacterial property of 316L-Cu stainless steel in different simulated body fluids. Mater Technol. 2021;36(2):118-30.
[20] Fadlallah SA, El-Bagoury N, El-Rab SMG, Ahmed RA, El-Ousamii G. An overview of NiTi shape memory alloy: corrosion resistance and antibacterial inhibition for dental application. J Alloys Compd. 2019;583:455-64.
[21] Gu KX, Wang KK, Zheng JP, Chen LB, Wang JJ. Electrochemical behavior of Ti-6Al-4V alloy in Hank's solution subjected to deep cryogenic treatment. Rare Met. 2018;1-10.
[22] Talha M, Behera CK, Sinha OP. Promising in vitro performances of nickel-free nitrogen containing stainless steels for orthopaedic applications. Bull Mater Sci. 2014;37(6):1321-30.
[23] Kim S, Kim G, Oh CY, Song S. Pitting and localized galvanic corrosion characteristics of gas tungsten arc welded austenitic stainless steel. Met Mater Int. 2022;1-14.